AD FALCON API Manual

Theory of the Unsaturated Generalized Cam-Clay Model

Javad Ghorbani

March 14, 2026

Contents

1 Theory of the Unsaturated Generalized Cam-Clay Model **3**
1.1 Syntax . . . 3
1.2 Material parameters . . . 3
1.3 Custom state variables . . . 5
1.4 Effective stress and suction-enhanced bonding . . . 5
1.4.1 Net and matric quantities . . . 5
1.4.2 Effective stress with saturation weighting . . . 6
1.5 Unsaturated state variable and cap hardening . . . 6
1.6 Yield surface and plastic potential . . . 7
1.7 Elasticity, consistency, and tangents . . . 8
1.8 Hysteretic soil–water retention curve . . . 10
1.9 Post-equilibrium state conditioning . . . 11
1.9.1 State-fitted initialization – `OCRControlled ≠ 1` . . . 11
1.9.2 Unsaturated `OCRControlled = 1` – Picard iteration . . . 12
1.10 Simulations . . . 12
1.10.1 Triaxial benchmarks - Saturated Case . . . 12
1.10.2 Input file . . . 12
1.10.3 Normally Consolidated Test . . . 14
1.10.4 Overconsolidated Test . . . 14
1.10.5 Highly Overconsolidated Test . . . 15
1.10.6 Unsaturated triaxial validation . . . 15
1.11 References . . . 15

1 Theory of the Unsaturated Generalized Cam-Clay Model

This theory note summarises the unsaturated Generalized Cam-Clay (GCC) formulation implemented in the accompanying UMAT, following Sheng et al. (2000) for the generalized yield surface, Gallipoli et al. (2003) and Borja (2004) for the suction-dependent state variable, and the hysteretic soil–water retention description of Ghorbani et al. (2018). The model bridges saturated Modified Cam-Clay (MCC) behaviour and suction-stiffened responses while remaining compatible with fully coupled hydro-mechanical finite elements.

1.1 Syntax

This model is configured in `% Materials` as a user-defined mechanical material. Use `@UMAT:` with category `Mechanical` and pass the parameters as `name=value` pairs.

Example:

```
@UMAT: path/to/GCCModel.cpp path/to/GCCModel.hpp Mechanical \
    Phi=30 Lambda=0.15 Kappa=0.03 Nu=0.25 Alpha=0.8 Beta_prime=1.0 \
    OCRControlled=1 DefaultIsoHardening=500 v_N=2.0 \
    P_min=0.1 patm=100 STOL=1e-5 FTOL=1e-6 LTOL=1e-6 \
    CustomVariable=IsotropicHardening,Delta_vN
```

For readability, this example is wrapped across multiple lines; in input files you should write the full `@UMAT:` directive on a single line.

Use the parameter names shown in the tables below.

1.2 Material parameters

Table 1. Material parameters and their descriptions

Symbol	Keyword in input	Units	Required	Description
ϕ'	`Phi`	°	✓	Critical-state friction angle.
λ	`Lambda`	–	✓	Virgin compression index (slope of NCL in v–$\ln p'$ space).
κ	`Kappa`	–	✓	Swelling/reloading index.
ν	`Nu`	–	✓	Poisson's ratio.

Symbol	Keyword in input	Units	Required	Description
α	`Alpha`	–	✓	Ratio M_c/M_e fixing Lode-angle dependence.
β'	`Beta_prime`	–	✓	Wet-side eccentricity ($\beta' \leq 1$ recovers MCC when $\beta' = 1$).
β	`Beta`	–	×	Optional eccentricity parameter (defaults to 1.0 when omitted).
c_1	`c1`	–	×	Optional suction-coupling coefficient (defaults to 0.0 when omitted).
c_2	`c2`	–	×	Optional suction-coupling coefficient (defaults to 0.0 when omitted).
v_N	`v_N`	–	✓	Specific volume at $p' = 1$ kPa on the saturated NCL.
$P_{\min}$	`P_min`	stress	✓	Lower bound applied inside the elastic bulk modulus.
p_{atm}	`patm`	stress	✓	Normalising pressure appearing in ζ.
`STOL`	`STOL`	–	✓	Stress integration tolerance for substepping.
`FTOL`	`FTOL`	–	✓	Yield-surface tolerance for return mapping / drift correction.
`LTOL`	`LTOL`	–	✓	Load–unload detection tolerance.

Symbol	Keyword in input	Units	Required	Description
a_0	`DefaultIso Hardening`	stress	✓	Minimum $\sigma_{mc0}^{\text{sat}}$ used in initialization.
OCRControlled	`OCRControlled`	–	✓	Initialization/conditioning mode selector (see below).
OBN	`OBN`	–	×	Optional overburden modifier (defaults to 0.0 when omitted).

1.3 Custom state variables

This UMAT uses custom state variables to store hardening-related quantities. Declare them using `CustomVariable=` in the `@UMAT:` line.

Name	Required	Meaning
`Isotropic Hardening`	✓	The saturated cap size / isotropic hardening variable.
`Delta_vN`	✓	Increment applied to `v_N` during conditioning (typically initialized to 0).
`OCR`	×	Required only for OCR-based conditioning modes; ignored otherwise.

Optional diagnostics (only if you include them in `CustomVariable=`):

- `PlasticStrainIncXX`, `PlasticStrainIncYY`, `PlasticStrainIncZZ`, `PlasticStrainIncZY`, `PlasticStrainIncZX`, `PlasticStrainIncXY` (declare these via `CustomVariable=` if you want them tracked and available for output)
- `NegDFailureFlag`, `BracketingFailureFlag`, `DriftFailureFlag`

1.4 Effective stress and suction-enhanced bonding

1.4.1 Net and matric quantities

Net stress and matric suction follow the tension-positive sign convention:

$$\boldsymbol{\sigma}_{\text{net}} = \boldsymbol{\sigma} + p_a \mathbf{I}, \qquad p_c = p_a - p_w \tag{1}$$

1.4.2 Effective stress with saturation weighting

Bishop's effective stress, written directly in terms of pore pressures and the degree of saturation, reads

$$\boldsymbol{\sigma}' = \boldsymbol{\sigma} - S_w\, p_w\, \mathbf{I} - (1 - S_w)\, p_a\, \mathbf{I} \tag{2}$$

The suction stress is obtained from the enriched Bishop coefficient $\chi(S_w)$,

> Note: The $\chi(S_w)$ weighting (and its parameters such as $\beta_{\chi,1}$ and $\beta_{\chi,2}$) is configured via your selected effective stress model, not via the GCC UMAT mechanical parameter list.

$$\chi(S_w) = S_w^{\left(\frac{\beta_{\chi,1}}{\beta_{\chi,2}}\right)}, \qquad \sigma_{\text{suc}} = \chi\, p_c \tag{3}$$

which recovers the classical $\chi = S_w$ when $\beta_{\chi,1} = 1$ and $\beta_{\chi,2} = 0$ used in the original model. Equations (1)–(3) apply throughout the mechanical formulation and in the suction-coupling terms.

1.5 Unsaturated state variable and cap hardening

The bonding variable ζ couples suction and saturation to the mechanical hardening law (Borja, 2004):

$$\zeta = \left(1 + \frac{p_c/p_{\text{atm}}}{10.7 + 2.4\, p_c/p_{\text{atm}}}\right)(1 - S_w) \tag{4}$$

Gallipoli et al. (2003) linked the current and saturated void ratios at the same stress level through

$$\frac{e}{e_{\text{sat}}} = 1 - c_1\,(1 - \exp(c_2 \zeta)) \tag{5}$$

with the corrected coefficient

$$\bar{c}_1 = c_1 \frac{e_{\text{sat}}}{1 + e_{\text{sat}}} \tag{6}$$

so that the ζ-dependent compressibility factor becomes

$$c_\zeta = 1 - \bar{c}_1\,(1 - \exp(c_2 \zeta)) = \frac{v}{v_{\text{sat}}} \tag{7}$$

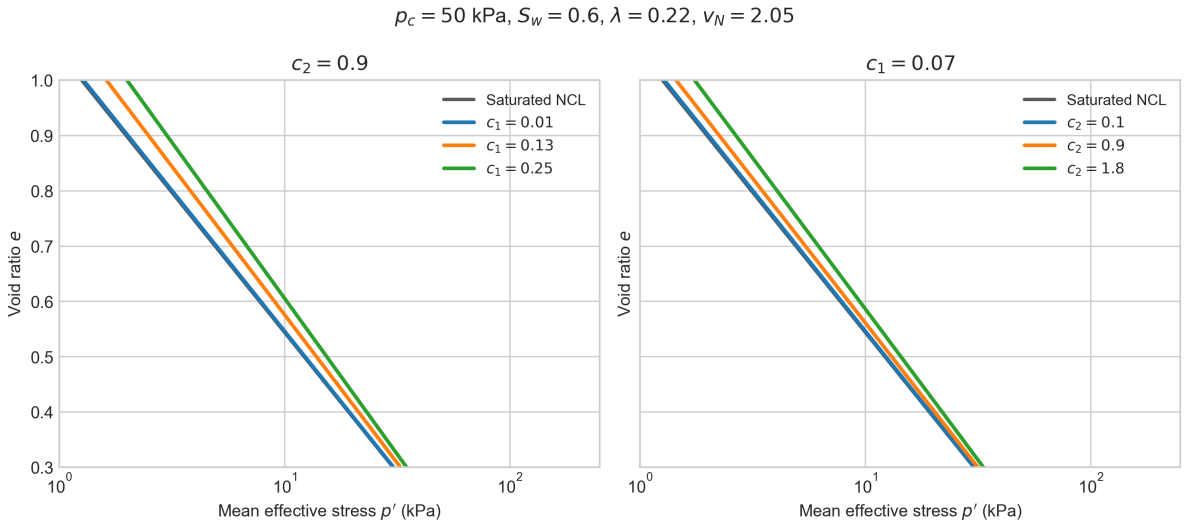

Figure 1: Influence of c_1 and c_2 on the unsaturated normal compression line

The unsaturated cap parameter, which sets the size of the yield surface, is related to the saturated value through

$$\sigma_{mc0}^{\text{unsat}} = \left(\sigma_{mc0}^{\text{sat}}\right)^{b_\zeta} \exp(a_\zeta) \tag{8}$$

where

$$a_\zeta = \frac{v_N(c_\zeta - 1)}{\lambda c_\zeta - \kappa}, \qquad b_\zeta = \frac{\lambda - \kappa}{\lambda c_\zeta - \kappa} \tag{9}$$

The specific volume at $p' = 1$ kPa, v_N, controls the intercept of the normal compression line (NCL), while λ and κ govern its slope and elastic unloading stiffness. Increasing c_1 deepens the intercept reduction, whereas c_2 amplifies the suction sensitivity, as illustrated in Figure 1. The plotted curves follow Equation (5) directly in e–p' space using a logarithmic stress axis between 1 and 250 kPa at a fixed suction state ($p_c = 50$ kPa, $S_w = 0.6$).

Figure 1. Stylised NCL shifts relative to the saturated line for different c_1 (left) and c_2 (right); curves are generated directly from Equation (5) in e–p' space with a log-scaled stress axis covering 1–250 kPa.

1.6 Yield surface and plastic potential

The generalized Cam-Clay yield function in p'–q–θ space reads

$$f = \frac{1}{\beta_{\text{side}}^2}\left(1 + \frac{(1+\beta')p'}{\sigma_{mc0}^{\text{unsat}}}\right)^2 + \left(\frac{(1+\beta')q\,F_\theta}{M\,\sigma_{mc0}^{\text{unsat}}}\right)^2 - 1 = 0 \tag{10}$$

with the Lode-angle modifier

$$F_\theta = \left[\frac{1 + \alpha^4 - (1 - \alpha^4)R_\theta}{2\alpha^4}\right]^{1/4} \tag{11}$$

and the third invariant ratio

$$R_\theta = -\frac{3\sqrt{3}\,J_3}{2J_2^{3/2}} \tag{12}$$

Here $M = 6\sin\phi'/(3 - \sin\phi')$ is the critical-state slope, and $\sigma_{mc0}^{\text{unsat}}$ sets the cap size. The eccentricity switches between the dry and wet sides through

$$\beta_{\text{side}} = \begin{cases} 1, & \text{(dry side) or } \beta' = 1 \\ \beta', & \text{(wet side) and } \beta' < 1 \end{cases} \tag{10a}$$

Equation (10a) therefore recovers the smooth Modified Cam-Clay ellipse ($\beta_{\text{side}} = 1$) on the dry side, whereas the wet side adopts the rounded GCC curvature ($\beta_{\text{side}} = \beta' \le 1$). The plastic potential shares the same structure (associated flow) unless a dilatancy correction is introduced. Figure 2 compares the two sides and highlights that only the wet branch is modified when $\beta' < 1$; the horizontal axis follows the tension-positive convention (compression at negative p') and only the compressive branch $q = Mp'$ is shown, with the vertical axis inverted to emphasise the negative q portion.

Figure 2. Numerical comparison of the MCC ($\beta' = 1$) and GCC ($\beta' = 0.45$) surfaces

---

1.7 Elasticity, consistency, and tangents

The elastic moduli follow isotropic linear elasticity with stress-dependent bulk stiffness:

$$K = \frac{v \cdot \max(P_{\min}, p')}{\kappa}, \qquad v = 1 + e \tag{13}$$

$$G = \frac{3(1 - 2\nu)}{2(1 + \nu)}K \tag{14}$$

$$\mathbf{D}^e = \begin{bmatrix} \lambda_e + 2\mu & \lambda_e & \lambda_e & 0 & 0 & 0 \\ \lambda_e & \lambda_e + 2\mu & \lambda_e & 0 & 0 & 0 \\ \lambda_e & \lambda_e & \lambda_e + 2\mu & 0 & 0 & 0 \\ 0 & 0 & 0 & \mu & 0 & 0 \\ 0 & 0 & 0 & 0 & \mu & 0 \\ 0 & 0 & 0 & 0 & 0 & \mu \end{bmatrix}, \quad \lambda_e = K - \tfrac{2}{3}G,\ \mu = G \tag{15}$$

Loading on the yield surface enforces the consistency condition

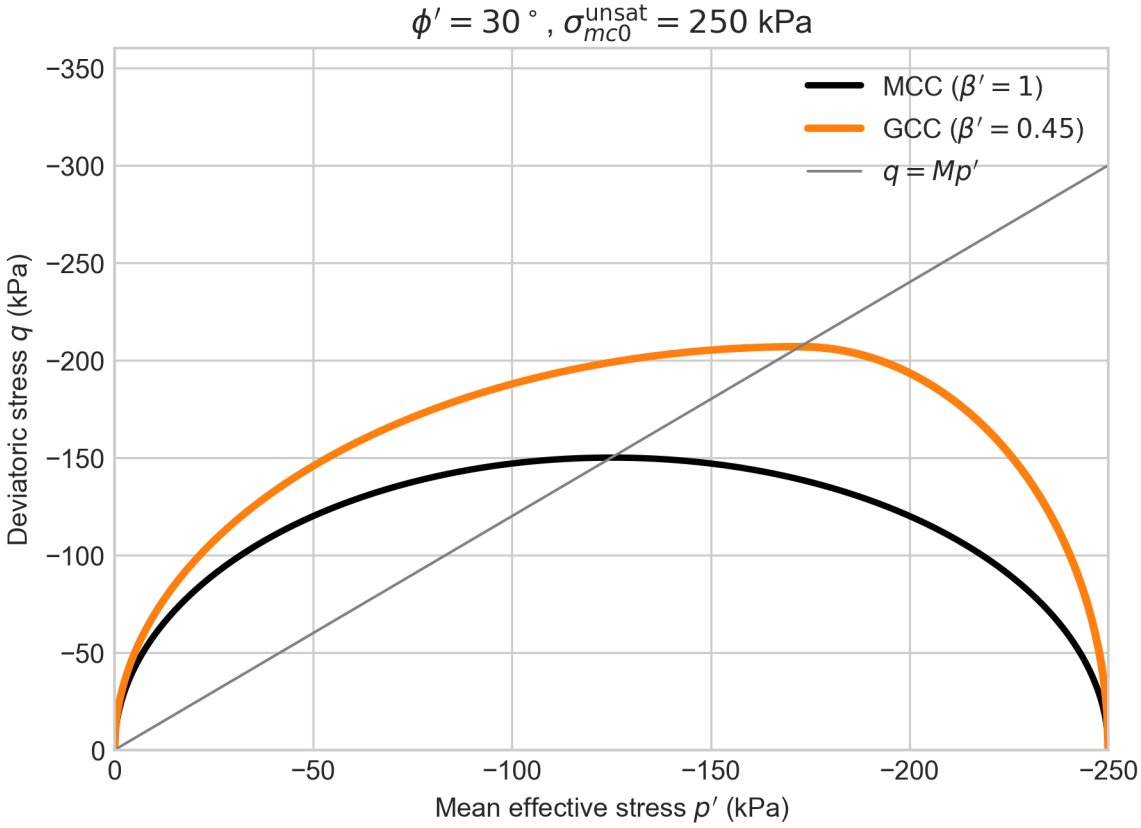

Figure 2: Smooth MCC and GCC yield surfaces in p'–q space

$$\frac{\partial f}{\partial \boldsymbol{\sigma}'} : d\boldsymbol{\sigma}' + \frac{\partial f}{\partial \zeta}\, d\zeta + \frac{\partial f}{\partial \sigma_{mc0}^{\text{unsat}}}\, d\sigma_{mc0}^{\text{unsat}} = 0 \tag{16}$$

with the elastic–plastic decomposition

$$d\boldsymbol{\sigma}' = \mathbf{D}^e \left(d\boldsymbol{\varepsilon} - d\lambda \frac{\partial g}{\partial \boldsymbol{\sigma}'} \right) \tag{17}$$

yielding the plastic multiplier

$$d\lambda = \frac{\dfrac{\partial f}{\partial \boldsymbol{\sigma}'} : \mathbf{D}^e d\boldsymbol{\varepsilon} + \dfrac{\partial f}{\partial \zeta} d\zeta}{K_p + \dfrac{\partial f}{\partial \boldsymbol{\sigma}'} : \mathbf{D}^e : \dfrac{\partial g}{\partial \boldsymbol{\sigma}'}} \tag{18}$$

where the hardening modulus is

$$K_p = -\frac{\partial f}{\partial \sigma_{mc0}^{\text{unsat}}} \cdot B_{\text{iso}}, \qquad B_{\text{iso}} = \frac{\partial g}{\partial p'} \frac{\partial \sigma_{mc0}^{\text{unsat}}}{\partial \varepsilon_v^p} \tag{19}$$

The elastoplastic constitutive update including suction coupling is

$$d\boldsymbol{\sigma}' = \mathbf{D}_{ep}\, d\boldsymbol{\varepsilon} + \mathbf{S}_{ep}\, dp_c \tag{20}$$

with

$$\mathbf{D}_{ep} = \mathbf{D}^e - \frac{\mathbf{D}^e \frac{\partial g}{\partial \boldsymbol{\sigma}'} \otimes \frac{\partial f}{\partial \boldsymbol{\sigma}'} \mathbf{D}^e}{K_p + \frac{\partial f}{\partial \boldsymbol{\sigma}'} : \mathbf{D}^e : \frac{\partial g}{\partial \boldsymbol{\sigma}'}} + \mathbf{S}_{ep}^{\varepsilon_v} \boldsymbol{m}^T \tag{21}$$

$$\mathbf{S}_{ep} = -\frac{\mathbf{D}^e \frac{\partial g}{\partial \boldsymbol{\sigma}'} \frac{\partial f}{\partial \zeta} \frac{\partial \zeta}{\partial p_c}}{K_p + \frac{\partial f}{\partial \boldsymbol{\sigma}'} : \mathbf{D}^e : \frac{\partial g}{\partial \boldsymbol{\sigma}'}} \tag{22}$$

$$\mathbf{S}_{ep}^{\varepsilon_v} = -\frac{\mathbf{D}^e \frac{\partial g}{\partial \boldsymbol{\sigma}'} \frac{\partial f}{\partial \zeta} \frac{\partial \zeta}{\partial \varepsilon_v}}{K_p + \frac{\partial f}{\partial \boldsymbol{\sigma}'} : \mathbf{D}^e : \frac{\partial g}{\partial \boldsymbol{\sigma}'}} \tag{23}$$

and $\boldsymbol{m} = [1, 1, 1, 0, 0, 0]^T$ is the volumetric projection vector. These consistent tangents feed directly into the finite-element stiffness and coupling matrices.

1.8 Hysteretic soil–water retention curve

The hysteretic soil–water retention formulation used by the GCC UMAT is documented in detail in `swrchys.md`. That note covers the modified suction definition, the van Genuchten main curves, the scanning-rule interpolation, and the void-ratio coupling that ties the hydraulic response back to the mechanical update.

1.9 Post-equilibrium state conditioning

After establishing stress equilibrium (e.g., following a geostatic initialization step), the model must ensure that the current stress state, void ratio, and hardening variables satisfy the consistency conditions of the elastoplastic framework. The `OCRControlled` flag selects how the initial cap stress (σ_{mc0}) and isotropic hardening variable are recovered from the equilibrium stress state to enforce compatibility between mechanical and hydraulic fields. Two branches are available:

- **`OCRControlled = 1`** – Used in **fully coupled unsaturated analyses**. A Picard-type iterative scheme maintains total stress constant while updating void ratio, saturation, and effective stress until convergence, ensuring consistency between the mechanical state and the hydraulic response.
- **`OCRControlled` $\neq$ `1`** – Available in **coupled saturated** and **uncoupled analyses only**. The current stress state is placed on the yield surface, and a prescribed offset (`DefaultIsoHardening`, `OCR`) defines the distance to the yield surface while ensuring the void ratio and cap size remain compatible with the elastoplastic formulation.

1.9.1 State-fitted initialization – `OCRControlled` $\neq$ `1`

Let the current effective stress invariants be p', q and F_θ the Lode-angle factor. The cap parameter on the saturated surface follows directly from the yield function,

$$f = \left(1 + \frac{(1+\beta')p'}{\sigma_{mc0}^{\text{sat}}}\right)^2 + \left(\frac{(1+\beta')q\,F_\theta}{M\,\sigma_{mc0}^{\text{sat}}}\right)^2 - 1 = 0 \tag{24}$$

with $Q = qF_\theta/M$. Two cases arise:

- **Dry side or** $\beta' = 1$

$$\sigma_{mc0}^{\text{sat}} = -\frac{p'^2 + Q^2}{p'} \tag{25}$$

- **Wet side with** $\beta' < 1$

$$\frac{1}{\beta'^2}\left(1 + \frac{p'}{\sigma_{mc0}^{\text{sat}}/(1+\beta')}\right)^2 + \left(\frac{Q}{\sigma_{mc0}^{\text{sat}}/(1+\beta')}\right)^2 = 1 \tag{26}$$

Introducing $x = (1+\beta')/\sigma_{mc0}^{\text{sat}}$ gives

$$\left[p'^2 + \beta'^2 Q^2\right] x^2 + 2p'x + (1-\beta'^2) = 0 \tag{27}$$

whose admissible solution is

$$\sigma_{mc0,-}^{\text{sat}} = \frac{(1+\beta')\left(p'^2 + \beta'^2 Q^2\right)}{-p' - \beta'\sqrt{p'^2 - (1-\beta'^2)Q^2}} \tag{28}$$

Once $\sigma_{mc0}^{\text{sat}}$ is known, the unsaturated cap follows from Equation (8). The OCR and default floor are applied via

$$\text{IsotropicHardening} = \max\left(\sigma_{mc0}^{\text{sat}} + \text{OCR} \times \text{DefaultIsoHardening},\ \sigma_{mc0}^{\text{sat}}\right) \tag{30}$$

`IsotropicHardening` always stores the saturated isotropic hardening variable. Unsaturated hardening values are not directly stored in FALCON and are obtained from the hydraulic state internally by the GCC UMAT.

1.9.2 Unsaturated `OCRControlled = 1` – Picard iteration

Maintaining the total stress σ_{tot} ensures that any change in void ratio, saturation, or suction feeds back consistently into the effective stress. A Picard loop enforces this coupling:

1. Initialize the void ratio from the supplied state and record σ_{tot}.
2. Compute $\sigma_{mc0}^{\text{sat}}$ from Equations (24)–(28), apply the chosen offset (Equations (30)–(31)), and recover $\sigma_{mc0}^{\text{unsat}}$ from Equation (8).
3. Update the void ratio, saturation, and effective stress from the new cap size.
4. Repeat until

$$\frac{|e_{\text{new}} - e_{\text{old}}|}{|e_{\text{old}} + 1|} < 10^{-5} \tag{32}$$

or the iteration limit (50 by default) is reached.

Regardless of the initialization branch, the void ratio is updated from the elastic NCL so that the specific volume remains compatible with the initialized `IsotropicHardening`,

$$v = v_N + \kappa\left(\ln(\text{IsotropicHardening}) - \ln(-p')\right) - \lambda \ln(\text{IsotropicHardening}), \qquad e = v - 1 \tag{37}$$

1.10 Simulations

1.10.1 Triaxial benchmarks - Saturated Case

1.10.2 Input file

```
# choose Undrained or Drained
Mode Drained

# material parameters
Phi 30
Lambda 0.077
Nu 0.3
Kappa 0.0066
Alpha 0.77
```

```
OCRControlled 2
DefaultIsoHardening 500
v_N 1.788
P_min 0.1
patm 100.0
STOL 1e-7
FTOL 1e-6
LTOL 1e-6

# initial state
VoidRatio 0.5
StressXX -100
StressYY -100
StressZZ -100

# saturation
DegreeOfSaturation 1.0
PoreAirPressure 0.0
PoreWaterPressure 0.0

# custom state
IsotropicHardening 500
OCR 0.0
Delta_vN 0.0

# control
dEpsAxial -0.0001
dQ_target -2.0
nSteps 2000
```

To confirm that our triaxial driver correctly reproduces the analytical benchmarks from Perić (2006), we ran three drained compression tests:

1. **Normally Consolidated (NC)**
   - **Setup:** Confining pressure $p_0 = 200$ kPa and isotropic hardening $\sigma_{mc0} = 200$ (kPa).

2. **Overconsolidated (OC)**
   - **Setup:** Confining pressure $p_0 = 100$ kPa with preconsolidation $\sigma_{mc0} = 200$ kPa.

3. **Highly Overconsolidated (HOC)**
   - **Setup:** $p_0 = 100$ kPa, $\sigma_{mc0} = 500$ kPa.

1.10.3 Normally Consolidated Test

Below are the three verification plots for the Normally Consolidated case (confining pressure $p_0 = \sigma_{mc0} = 200$ kPa). From left to right:

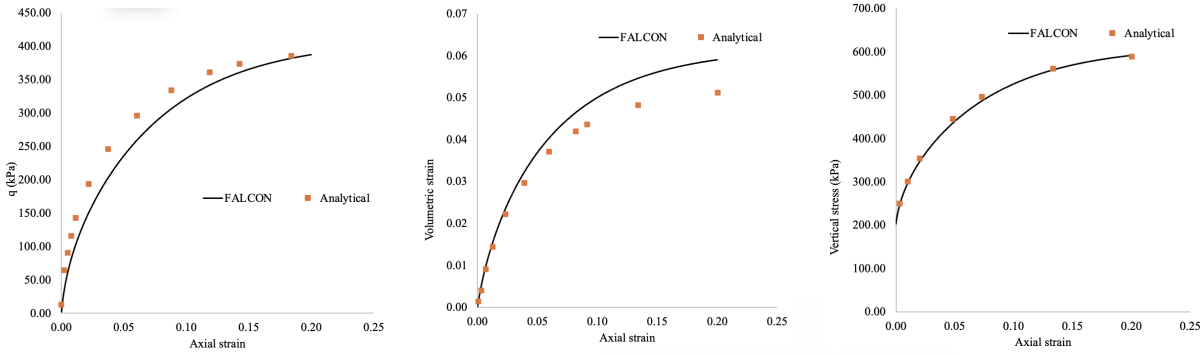

(1) Deviatoric Stress q vs. Axial Strain	(2) Volumetric Strain vs. Axial Strain	(3) Vertical Stress σ_1 vs. Axial Strain

Figure 3. Normally consolidated test results ($p_0 = \sigma_{mc0} = 200$ kPa): (1) deviatoric stress vs. axial strain, (2) volumetric strain vs. axial strain, and (3) vertical stress vs. axial strain.

1.10.4 Overconsolidated Test

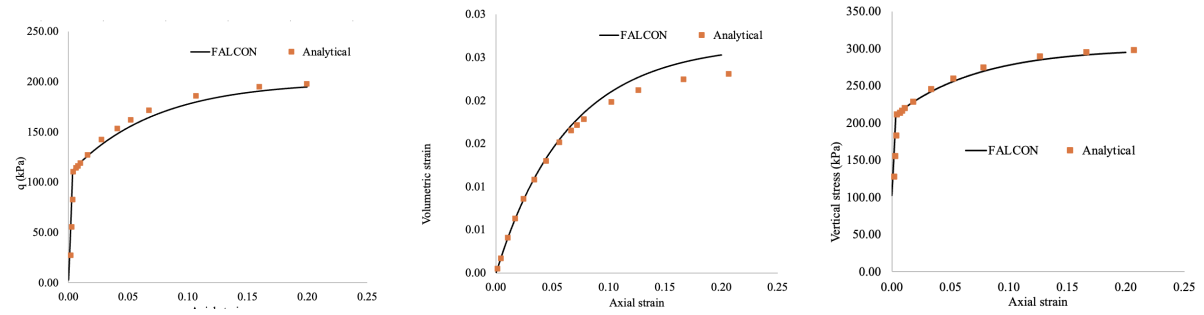

(1) q vs. Axial Strain	(2) Volumetric Strain vs. Axial Strain	(3) σ_1 vs. Axial Strain

Figure 4. Overconsolidated test results ($p_0 = 100$ kPa, $\sigma_{mc0} = 200$ kPa): (1) deviatoric stress vs. axial strain, (2) volumetric strain vs. axial strain, and (3) vertical stress vs. axial strain.

1.10.5 Highly Overconsolidated Test

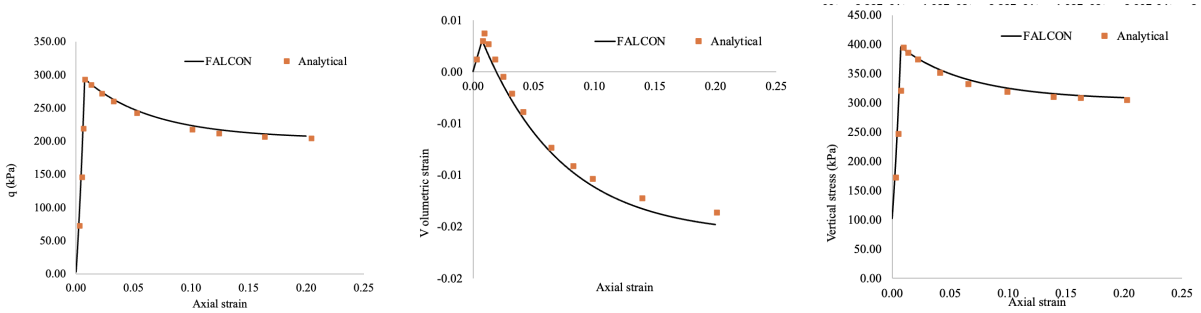

(1) q vs. Axial Strain	(2) Volumetric Strain vs. Axial Strain	(3) σ_1 vs. Axial Strain

Figure 5. Highly overconsolidated test results ($p_0 = 100$ kPa, $\sigma_{mc0} = 500$ kPa): (1) deviatoric stress vs. axial strain, (2) volumetric strain vs. axial strain, and (3) vertical stress vs. axial strain.

1.10.6 Unsaturated triaxial validation

We repeated the simulations under constant suctions to mirror the GCC verification campaign. Each case follows a drained path with $dq/dp_{\text{net}} = 3$ starting from $\sigma_{xx} = \sigma_{yy} = \sigma_{zz} = -100$ kPa. Common parameters are:

- $\phi = 25^\circ$, $\lambda = 0.11$, $\kappa = 0.03$, $\nu = 0.30$, $v_N = 2.76$, $\beta = \beta' = 1.0$.
- Unsaturated coupling: $c_1 = 0.20$, $c_2 = 1.50$, $\Omega' = 0.2$, $e_0 = 1.5$, $\sigma_{mc0}^{\text{sat}} = 100$ kPa.
- Initialization Option 2 with $a_0 = 2.0$ kPa, tolerances STOL $= 10^{-9}$, FTOL $= 10^{-9}$, LTOL $= 10^{-6}$.

The suction levels were $p_c = 0$ kPa (saturated), $p_c = 5$ kPa, and $p_c = 10$ kPa. As suction increases, $\sigma_{mc0}^{\text{unsat}}$ grows and the response shifts from net compaction toward pronounced dilation.

Figure 6. Deviatoric stress and void-ratio histories under constant suction with $dq/dp_{net} = 3$; higher suction stiffens the response and drives dilation.

1.11 References

- **Borja (2004)**: Borja, R. I. (2004). *Cam-Clay plasticity. Part V: A mathematical framework for three-phase deformation and strain localization analyses of partially saturated porous media.* Computer Methods in Applied Mechanics and Engineering, 193(48-51), 5301–5338.

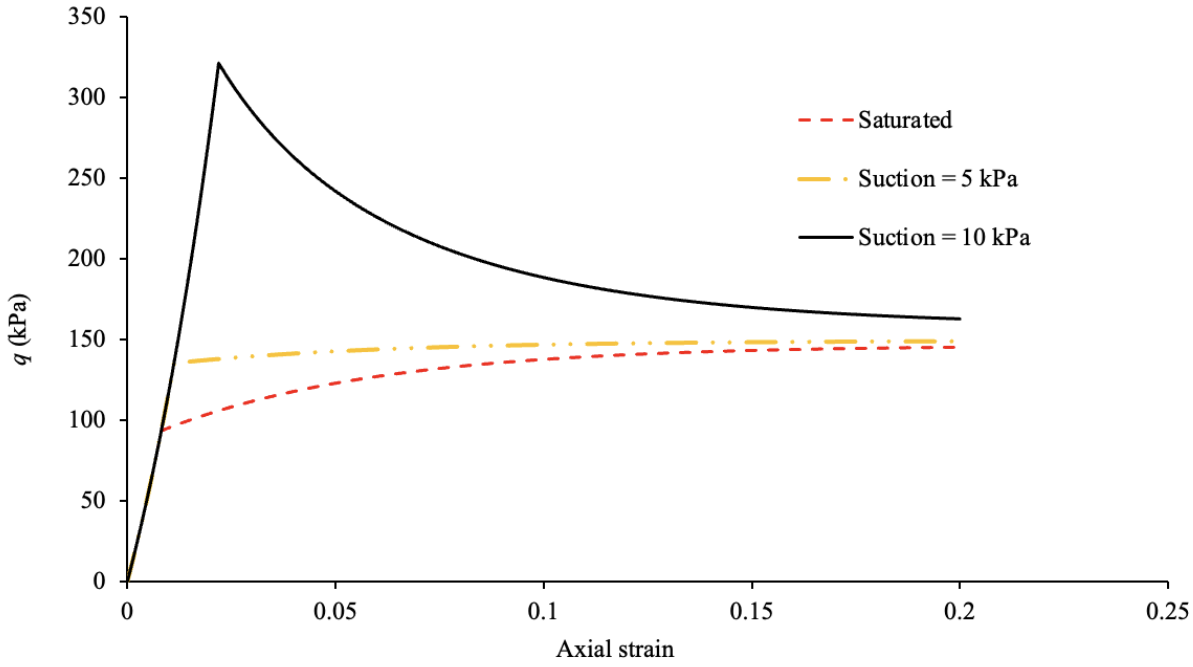

Figure 3: Drained unsaturated triaxial simulations at constant suction

- **Gallipoli et al. (2003)**: Gallipoli, D., Gens, A., Sharma, R., & Vaunat, J. (2003). *An elasto-plastic model for unsaturated soil incorporating the effects of suction and degree of saturation on mechanical behaviour.* Géotechnique, 53(1), 123–135.
- **Ghorbani et al. (2018)**: Ghorbani, J., Airey, D. W., & El-Zein, A. (2018). *Numerical framework for considering the dependency of SWCCs on volume changes and their hysteretic responses in modelling elasto-plastic response of unsaturated soils.* Computer Methods in Applied Mechanics and Engineering, 336, 80–110.
- **Ghorbani & Kodikara (2024)**: Ghorbani, J., & Kodikara, J. (2024). *Thermodynamically consistent effective stress formulation for unsaturated soils across a wide range of soil saturation.* Computational Mechanics, 73(5), 1077–1094.
- **Perić (2006)**: Perić, D. (2006). *Analytical solutions for a three-invariant Cam clay model subjected to drained loading histories.* International Journal for Numerical and Analytical Methods in Geomechanics, 30, 363–387.
- **Sheng et al. (2000)**: Sheng, D., Sloan, S. W., & Yu, H. S. (2000). *Aspects of finite element implementation of critical state models.* Computational Mechanics, 26(2), 185–196.